Journal of the Iranian Chemical Society (2019) 16:2081–2092
https://doi.org/10.1007/s13738-019-01678-3

ORIGINAL PAPER

Dual-emission carbon dots as biocompatible nanocarrier for in vitro/in vivo cell microenvironment ratiometric pH sensing in broad range

Somayeh Hamd-Ghadareh[1,2] · Abdollah Salimi[1,2] · Fardin Fathi[3] · Farzad Soleimani[3]

Received: 21 January 2019 / Accepted: 15 April 2019 / Published online: 19 April 2019

Abstract

Herein, dual-emission carbon dots (CDs) were facilely prepared, CDs have a narrow size distribution, and the mean particle size is about 3.5 nm. CDs exhibit good water dispersibility and can emit intense green fluorescence under 365 nm UV light in an aqueous solution, which can be stable in different conditions. CDs used as ultrabright fluorescent probes for highly sensitive self-monitoring of pH on account of ratio of dual fluorescence intensities (I_{336} nm/I_{540} nm) against the pH variation from 2.5 to 12.0. The CDs exhibit cell permeable properties and a distinct pH-sensitive/excitation-independent PL emission feature, yielding significantly an optical probe for intracellular pH sensing and multicolor imaging of live HeLa and MDA-MB-231 cells with micron lateral resolution. Besides, MTT assay revealed the cell viability did not change upon treatment with CDs probe during 36 h.

Keywords Ratiometric · Carbon dots · pH sensing · In vitro/in vivo cellular barcoding · HeLa and MDA-MB-231 cell bioimaging

Introduction

Carbon dots (CDs) as an important class of zero-dimensional photoluminescence (PL) nanomaterials in carbon family comprise a strongly fluorescent, non-toxic, non-blinking, oxygenous carbon nanoparticles and have been the subject of extensive research over the past decade with great analytical and bioanalytical potential [1–7]. On account of inherent advantages such as low cost, reduced toxicity, and excellent biocompatibility [5–8], number of researches based on CDs usance drastically increased. In the context of analytical chemistry, by controlling the functionalization step a specific chemical reactivity of the nanoparticle allows it to act as a chemical sensor [8, 9]. Instance, CDs in most literatures just have blue fluorescence, which substantially limit their applications and developments owing to the general blue autofluorescence of biological substrate and photo-damage of biotic organization under UV excitation light [10]. By contrary, green and red emissive CDs are advantageous for their applications, especially in the biomedical fields, which show low tissues damage in organizations [11]. Conventional fluorescent strategies principally were based on measuring the absolute increase or decrease in the intensity changes of a solely responsive signal which was readily perturbed by numerous experimental conditions, including [12, 13] environment (such as temperature and pH), the influence of the sample concentration, equipment effects (like photobleaching and background light), and other factors.

Surprisingly, on account of self-calibration capability, ratiometric fluorescent measurement [14–17] is able to cancel out environmental fluctuations and provides an intrinsic rectification for external interference, specially terminating fluctuations of the excitation light intensity by calculating emission intensity ratio at two different wavelengths [15–19].

Recently, optical tracking of pH, especially, using fluorescence probes has been the subject of extensive research

Electronic supplementary material The online version of this article (https://doi.org/10.1007/s13738-019-01678-3) contains supplementary material, which is available to authorized users.

✉ Abdollah Salimi
absalimi@uok.ac.ir; absalimi@yahoo.com

[1] Department of Chemistry, University of Kurdistan, Sanandaj 66177-15175, Iran

[2] Research Center for Nanotechnology, University of Kurdistan, Sanandaj 66177-15175, Iran

[3] Cellular and Molecular Research Center, Kurdistan University of Medical Sciences, Sanandaj 66177-13446, Iran

[20–26] over the other methodologies due to high sensitivity, intrinsic selectivity and the distinct capacity for rapid, real-time monitoring advantages of fluorescence probes [24–34]. Furthermore, pH monitoring inside living cells is very important for investigating physiological and pathological processes, because intracellular pH has an influential role in many essential biological processes; specially it is vital in early cancer theranostic [33–41].

Herein, in continuation of our recent study for synthesis and applications of carbon dots for sensing/biosensing of various biomarkers and bioimaging of different cells [2, 42–44], we report successful preparation of a dual PL emission CDs. The proposed CDs were synthesized based on hydrothermal reaction at 60 °C using hydroquinone, ethylenediamine and ammonium as precursors. The resulting CDs show not only fluorescence emissions at two dominant locations under different excitation wavelengths, but also two emission peaks under a single excitation wavelength are observed. Interestingly, these two emission peaks respond to pH changes relatively with opposite tendency, which enables the prepared CDs to be a potential ratiometric probe for pH sensing without the necessity to integrate with other fluorescent dyes. This ratiometric fluorescent pH-probe was able to cancel out environmental fluctuations by tracking emission intensity ratio at two distinct wavelengths, being robust and stable enough for detection of pH. We examined the feasibility of using excitation-independent PL CDs to construct a ratiometric fluorescence assay for HeLa and MDA-MB-231 cell multicolor imaging in both in vitro and in vivo cellular imaging.

Experimental

Materials

All chemicals are from commercial sources and are of analytical grade. Chemicals including ammonium oxalate, hydroquinone, and ethylenediamine were obtained from Sigma-Aldrich without further purifications. The dialysis membrane with molecular weight cutoff (MWCO) 1 kDa was acquired from Fisher Scientific. Reagents for cell culture, Dulbecco's Modified Eagle Medium (DMEM), Minimum Essential Medium Eagle (MEM) and fetal calf serum were purchased from Life Technologies Holding Pte Ltd. Acetone, methanol, Ethanol and 3-(4,5-dimethylthiazol-2-yl)-2,5-diphenyl tetrazolium bromide (MTT) were acquired from Sinopharm Chemical Reagent Co., Ltd.

Apparatus

Optical absorption and emission measurements were taken on stirred CDs solutions. Optical absorption spectra were measured with a Varian Cary 5000 UV–Vis–NIR absorption spectrometer, Agilent Technologies, USA. Fluorescent emission and excitation spectra were measured on a Varian Cary Eclipse Fluorescence Spectrophotometer, Agilent, USA, at ambient conditions. Fourier transform infrared (FTIR) spectra were obtained on a Bruker Tensor 27 spectrometer (Bruker, Karlsruhe, Germany) using KBr pellets prepared from the samples. Transmission electron microscopy (TEM) and high-resolution TEM (HR-TEM) observations were performed on a Tecnai F20 microscope. X-ray photoelectron spectroscopy (XPS) was performed on an Thermo Scientific ESCALAB 250 spectrograph with Al/Kα as the source. Binding energy calibration was based on C1s at 284.6 Ev. All pH measurements were taken with a basic pH meter PB-10 (Sartorius Scientific Instruments Co., Ltd., Beijing, China). The absorbance for 3-(4,5-dimethylthiazol-2-yl)-2,5-diphenyltetrazolium bromide (MTT) assay was carried out using a Tecan's Infinite M200 microplate reader at wavelength of 490 nm.

Synthesis of CDs

In a typical experiment, 0.5 g of hydroquinone and 0.5 g of ammonium oxalate were added to 10 mL of water and rapidly dissolved to form clean homogeneous solution and then 500 µL ethylenediamine droplets were added to the solution under vigorous stirring for 3.0 h (a pale yellow saffron colored solution). Then 1.0 mL H_2SO_4 was added to the solution after being heated at a 60 °C for another 7.0 h. The mixture was then transferred into a 50 mL Teflon-lined autoclave. After being heated at a 180 °C for 12 h, the autoclave was cooled down to room temperature naturally. The room-temperature-cooled CDs solution was collected from supernatant by extracting the large dots over centrifugation. Consequently, the small carbogenic nanoparticles were acquired after being purified by dialyzing against deionized water via a dialysis membrane for 24 h to pull out the extra precursors. The suspension seemed homogeneous saffron and was freeze-dried until powder and reserved in the dark for more characterization and usage. The influence of carbon source precursor and various parameter affecting the CDs PL properties is investigated as follow.

Optimization of CDs synthesis condition

A series of isomers including small oxygenous aromatic benzenediol (catechol (o-$C_6H_6O_2$), resorcinol (m-$C_6H_6O_2$) and hydroquinone (p-$C_6H_6O_2$), respectively) were selected as the carbon precursor for the fabrication of CDs. The hydrothermal-assisted method is a comparably easier way to perform, if assisted with specialized reaction precursors in advance. As reported in earlier studies, sulfuric acid was used as dehydrator in the hydrothermal heating reaction. In order

to find the efficient volume of H_2SO_4 (0.25 mL, 0.5 mL, 0.75 mL, 1.0 mL and 1.5 mL) were added into a solution of 0.5 g of benzenediol isomers in 10 mL H_2O. Between different H_2SO_4 volumes, 1.0 mL resulted high-quality fluorescent CDs. Then the small carbogenic nanoparticles were obtained after being purified by dialyzing against deionized water through a dialysis membrane for 24 h to remove the excess precursors. After hydrothermal-assisted heating, the color of the mixture solution turned to yellow saffron or dark green (under UV illumination), indicating the formation of CDs [31]. Some other acids like nitric acid, phosphoric acid and hydrochloric acid were also tried as the catalyst instead of sulfuric acid. Considering the optical characteristics in term of emission wavelength position, the same fluorescent product was only observed in the one with phosphoric acid. But, He quantum yield of product using phosphoric acid (12%) as catalyst was not as much as that using sulfuric acid (29%). Then, the effect of reaction time on the preparation of CDs was investigated. For simple mixing reaction of precursors at 60 °C 10 h and more showed the same results, so 10 h used in continue. All of the produced CDs that showed two distinct and excitation-independent emission characteristics PL spectra for benzenediol series are different in peak position and shape despite a little, detailed information listed in Table S1. After dialysis of the resultant synthesis solution, the output of p-CDs (hydroquinone--derived CDs) was used for characteristics and analysis.

Cell cultures

HeLa and MDA-MB-231 cells were cultured in cell culture flasks containing Dulbecco's modified Eagle's medium with 10% fetal bovine serum, 100 U mL^{-1} penicillin, 100 μg mL^{-1} streptomycin, and 100 U mL^{-1} L-glutamine. Culture flasks were maintained in a humidified incubator at 37 °C with 5% CO_2. When at confluence, HeLa and MDA-MB-231 cells were enzymatically dispersed using trypsin-ethylenediamine tetra acetic acid (EDTA) and then plated on the different polymer substrates at a concentration of 20 000 cells cm^{-2}. Cells were fixed for 20 min at room temperature in 4% paraformaldehyde and 4% sucrose in 0.12 M sodium phosphate buffer, pH 7.4.

Cytotoxicity investigation of CDs

Before pH monitoring experiments, we evaluated the cytotoxicity of CDs by performing the (MTT) assay on the HeLa cells after 12, 24, and 48 h of incubation with and without the CDs. HeLa cells were seeded in a 96-well plate that contained Dulbecco's modified Eagle's medium (DMEM) supplemented with 10% fetal bovine serum (FBS, invitrogen). The cells were cultured first for 24 h in a humidified atmosphere containing 5% CO_2 at 37 °C. Then, different concentrations of the CDs solution were added into each well, followed by incubation for 24 h. PBS buffer was used to wash samples three times and then every cell well received fresh culture medium containing 20 μL MTT (5 mg mL^{-1}), followed by an additional 4-h incubation period. The culture medium was then removed, and the obtained mixtures were dissolved in 100 μL DMSO and shaken for 10 min. A Microplate Reader Model was used to measure the optical density (OD) of the mixture at 450 nm.

Fluorescence measurement and bioimaging of HeLa and MDA-MB-231 cells

To investigate the pH-sensitive behavior of CDs, 20 μL of the freshly prepared CDs solution (0.05 mg mL^{-1}, 5 mL) was diluted by 5 mL double distilled water, and PL was measured. HCl (2 M) or NaOH (2 M) was used to adjust the pH of the resultant CD aqueous solution; then, the fluorescence spectra of the mixture were recorded after equilibrated mixed solution for 5 min through vibrating. 300 μL quartz cell with a 1 cm of optical length was employed for the fluorescence measurement under the excitation of 310 nm. The titration curve of ratiometric signals ($R = I_{336}/I_{540}$) versus pH values was plotted. In order to evaluate the reversibility of the resultant CDs, the solution pH was assorted between 4.0 and 11.0 in a cyclic mode, and the intensity ratios were calculated.

HeLa cells were grown in Dulbecco's Modified Eagle's Medium (DMEM) cell culture medium containing 10% fetal bovine serum, penicillin (100 U mL^{-1}), and streptomycin (100 mg mL^{-1}) under a humidified atmosphere with 5% CO_2 at 37 °C. For the pH bioimaging, cells were plated into 96-well plate at 37 °C for 1 day. After they washed with PBS (0.1 M, pH 7.4), for in vitro HeLa bioimaging, the cells were fixed with 4% paraformaldehyde at room temperature for 10 min. Afterward, formaldehyde was removed and the cells were again washed with PBS and allowed to incubate with 10 μL of CDs solution with distinct pH for 20 min. Thereafter, the adhered cells were washed thrice with PBS to remove the CDs that were not taken up into the cells. The multicolor imaging of nanosensor loaded cells was simultaneously collected from blue channel (FITC), green channel (the oxidation product of HE), and red channel (SiO2@QD) in the wavelength ranges of 510–570, 600–670, and 730–800 nm, respectively.

For live HeLa and MDA-MB-231 cells, they were seeded at a density of 1×10^4 cells per well into 96-well microtiter plates, and grown in high glucose Dulbecco's Modified Eagle's Medium supplemented with 10% fetal bovine serum, 80 μg mL^{-1} streptomycin, and 80 U mL^{-1} penicillin. After being incubated at 37 °C under 5% CO_2 for 24 h, the culture media was replaced with fresh one containing the CDs (0.05 mg mL^{-1}) and further cultivated for 30 min. Three

replicate experiments were performed for each value. The applicability of proposed CDs for in vitro ratiometric sensing was investigated by internalizing carbon dots into HeLa cells and their PL monitoring as a function of the intracellular pH using confocal fluorescence microscopy.

Results and discussion

Physicochemical characterization

The preparation of CDs was conducted in aqueous solution medium; first, polymer-like CDs were formed; then, they converted to carbonized CDs with high photoluminescent activity. As it is obvious from Fig. 1a, CDs are in spherical shape with an average size of ~ 3.5 nm (Fig. 1a, inset) and the particle size distribution is in the range of 2.0–6.0 nm (Fig. 1a, Inset). Furthermore, the selected area electron-diffraction (SAED) result (Fig. 1b) corresponded to the high crystallinity and displayed a ring pattern. Furthermore, we demonstrated the significant impact of such fluorophores nanostructures on the optical properties of CDs and revealed their footprint by studying the excitation-independent emission characteristics and the trends in CDs 2D PL plots. Particularly, the emission spectra of an aqueous solution of the CDs are featured of λex independent fluorescence (Fig. 1c), showing dual, narrow, and nearly symmetric peaks at 336 and 540 nm with the maximum intensity at λex 270 and excitation of 430 nm for 540 nm emission. This highlights that the emission in CDs arises from two emission centers, (1) the surface groups localized in CDs surface are dominant (second emission band at 540 nm), (2) while the core ascribed emission (336 nm) in encapsulated structure with lower intensity. The optimum emissive center of CD sample remains at 336 and 540 nm under 310 nm excitation. In order to investigate the origin of fluorescence in CDs and confirm the luminescent center of CDs, specified 2D fluorescent matrix scan was performed (Fig. 1c, d) in aqueous and acetonitrile as solvents with different polarities.

As it is clear from Fig. 1c, d, dual emissions of CDs are related with an identical phenomenon. Based on the 2D fluorescent map, a symmetric ellipse area of core which is encapsulated in matrix region produces the first emission. The second fluorescent center at 540 nm with an emission tail into longer wavelength is assigned to the intrinsic energy level of N-related defect state between surface bands [33]; this phenomenon was observed in acetonitrile as other investigated solvents.

The FTIR spectroscopy of synthesized CDs confirmed the presence of the oxygen-containing groups (O–H, –COO–, C–O, C=O, epoxy), C – H, C = C along with the nitrogen-containing, heteroatom-bound N–H and N–C groups in the

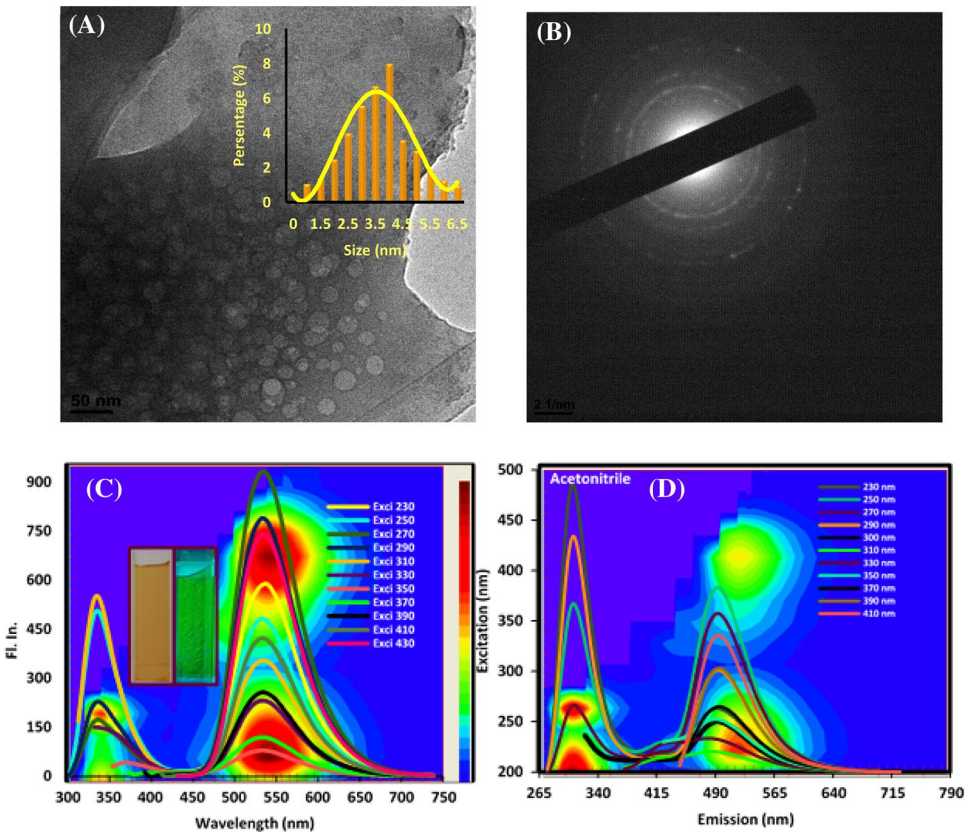

Fig. 1 **a** HR-TEM image of the CDs and the particles size distribution histogram (inset). **b** The selected area electron-diffraction (SAED) result pattern, **c**, **d** PL spectra and 2D fluorescent matrix scan of CDs in H_2O and acetonitrile solvents

surface state and chemical framework of the CDs (Figure S1A). Detailed information was reported in ESI. Figure S1B shows the absorption, excitation and PL emission spectra of CDs. The main absorption peak centered at 243 and 282 nm with highest energy level (sp^2 carbogenic network) is well fitted with π–π* transitions of the graphitic "core state" [34–37]. The second and third absorption band centered at 341 nm (n–π* transition of carbonyl groups) is assigned to n–π* transition arising from edge transition of CDs. The "edge band" of CDs was reported in most cases before, which refers to those atoms at the edge within the crystallized carbon core, especially in some blue emitting CDs [37]. The third broad absorption band arises from 453 nm and extends to longer wavelength composed of a group of low energy absorption tail bands. It is considered as the "surface band" of CDs due to the adherence of functional groups to the edge [34]. Likewise, the emission spectrum can be mainly divided into two areas. At the same time, the first fluorescent center of CD comes out when the excitation descends to ~ 300 nm, corresponding to π–π* transition from core state in CD. Figure S1C shows the normalized PL spectra for CDs, as it is obvious the PL centers are excitation independent. Thus, the existence of multiple fluorescent centers in PL plot starts giving rise to a possibility of multi-excitation options for the acquisition of expected luminescence. The CDs can be tentatively considered to be composed of dual-emission centers, one which covering UV region and the other localized in visible region. In the X-ray photoelectron spectroscopy survey (Fig. 2a–d) of the CDs observed three peaks at 284.0, 401.0 and 533 eV are considered as the C1s, N1s and O1s binding peak, respectively [38]. Detailed information was reported in ESI.

Optical properties of CDs and their application in ratiometric pH sensing

The excitation-independent green emission PL property makes CDs product very potent in fabricating sensing systems with a wide range of applications. The PL properties should be calibrated, so we first investigate the sensitivity and robustness of the CDs solution products toward pH variations. Fluorescent spectra of CDs with two emission wavelengths at different pHs were recorded under 310 nm excitation wavelength. Changes in intensity (I_{336} nm/I_{540} nm) can serve as ratiometric probes for microenvironment monitoring of the pHs levels with high sensitivity (Fig. 2e, f).

In contrast to most of the reported nanomaterial-based ratiometric pH sensors which count on the coupling of additional dyes, these CD-based ratiometric probes were free from labels. However, it may be deducing that the

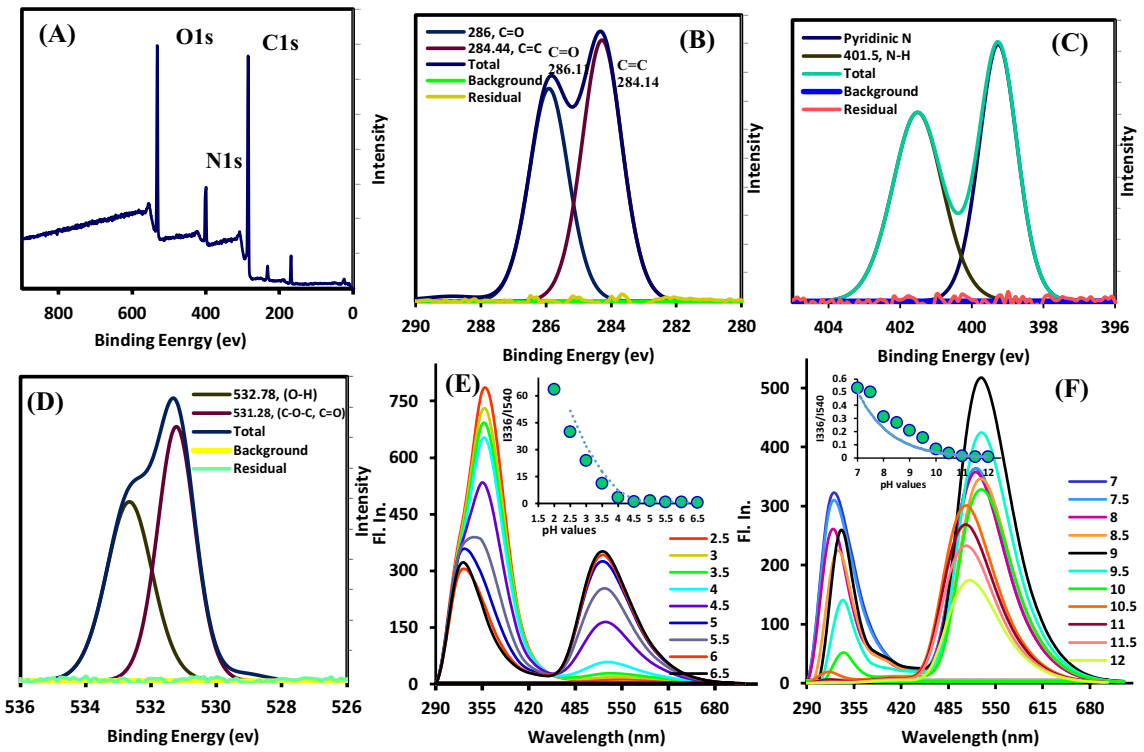

Fig. 2 Entire XPS scanning spectrum of the CDs. Survey scan (**a**), the high-resolution C 1s (**b**), N 1s (**c**), and O 1s (**d**) XPS spectra. PL spectra of the CDs in aqueous solution as a function of pH (**e**) from 2.5 to 7.5 and (**f**) from 8.0 to 12.0 (insets of **e** and **f**) are total PL changes for CDs versus pHs values upon titration with HCl and NaOH from 2.5 to 7.5 and 8.0 to 12.0, respectively, at λex = 310 nm

emission in UV region is probably not from CDs but from the molecular precursors; to clarify the origin of this emission, we investigate the emission of precursors; the results showed that there is no PL emission for dihydroxybenzenes and showed that CDs with dual emission formed through a thermal reaction. Also, purification of CDs by dialyzing against deionized water through a dialysis membrane was conducted for 24 h to remove any molecular species such as the molecular precursors and molecular intermediate during the synthesis. Also, the PL spectra of molecular precursors screened for comparison to explore the distinct origin for UV-emission.

Both of the emissions at 336 and 540 nm were appeared when CDs excited at 310 nm. These dual emissions were pH sensitive, and then we applied this novel kind of label-free CDs for intracellular ratiometric fluorescence pH sensing. Furthermore, the PL emission of CDs nanoprobe at whole interval divided into two distinct regions as illustrated in Fig. 2e, f. The emission peak position (336, and 540 nm) remained almost unchanged; however, the PL intensities are found to be significantly altered with pH. The distinct PL emission of CDs nanoprobe at distinct analytical pH includes 3.5, 6.5 and 10.5 represented in Figure S2A. Figure S2B illustrates the ratiometric total PL changes for CDs versus pH values from 2.5 to 12.0 at $\lambda ex = 310$ nm. Furthermore, the colorimetric profile of CDs solution at five distinct pHs under UV illumination is shown in Figure S2C. The clear and well mature PL emission for produced CDs was observed in UV region for all benzenediol isomers showed CDs with dual emissions formed successfully (Fig. 3).

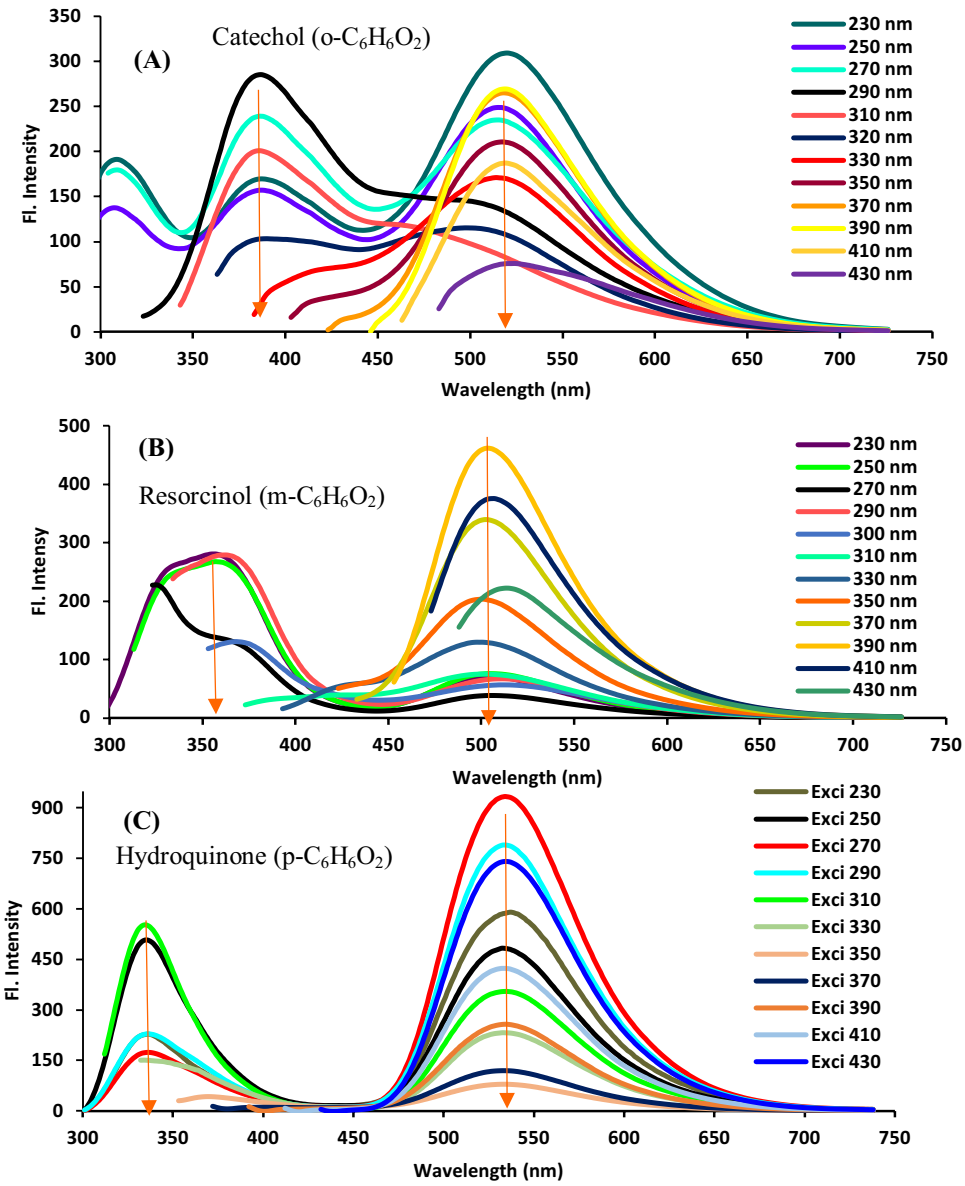

Fig. 3 PL spectra for benzenediol derived CDs at different excitation wavelengths

The effects of temperature, photoradiation and ionic strengths on PL stability of CDs

The long-term stability of the CDs solution was investigated with pH titration of the sample after 4 months of shelf time. The data show no evident aging effect on the CDs pH sensitivity. So, due to high stability of CDs in polar environment, their ability for ratiometric pH sensing was evaluated. The fluorescence intensities of the as-prepared CDs toward extreme pH, temperature, high ionic strengths in solution and illumination with a Xe lamp were measured (Figure S3 (A, B, C). The PL intensity of CDs was almost unchanged under continuous excitation of at least 30 min with a Xe lamp or being kept for 4 months at room temperature, which demonstrates the excellent photostability of these CDs (Figure S3-A). The influence of different ionic strengths on the PL intensity of CDs was evaluated in NaCl solution with varying concentrations from 0 to 1.0 M. As shown in Figure S3-B, the high stability of the CDs even under extreme ionic-strength conditions to use these CDs in salt solutions such as buffers will be beneficial.

The effect of temperature on the PL properties of CDs was also investigated in aqueous solution from 5 to 50 °C (Figure S3-C). The temperature-induced PL quenching results were suggested to be highly related to the enhanced nonradiative relaxation. More details reported in SI file. In Fig. 4a, B the digital photograph of CDs solution in normal light and under UV illumination shows this color changes more clearly. To investigate the pH-sensitive behavior of the prepared CDs, the solution pH was assorted between 4.0 and 11.0 in a cyclic mode and the intensity ratios were determined. The CDs also displayed excellent reversibility and photostability during pH change, indicating robustness and sensitivity of these CDs against extreme pH fluctuations (Fig. 4c), due to stability and inherent characteristic of fast protonation/deprotonation process of CDs as fluorescent probe. Meanwhile, the color of the CDs aqueous solution along with pH variations shows drastic changes, it is darkened in strong acidic pH, and then showed light yellow saffron color in middle pH; then by increasing the pH to basic region the light yellow saffron turned to yellow brown gradually. The pH dependent properties may be attributed to aggregation of the synthesized CDs by their surrounding carboxyl groups at lower pH, resulting in the fluorescence quenching for surface-related emission band. This phenomenon also confirms that the hydrophilic carboxyl groups are present on the surface of N-doped CDs. Also this phenomenon may confirm the reversibility

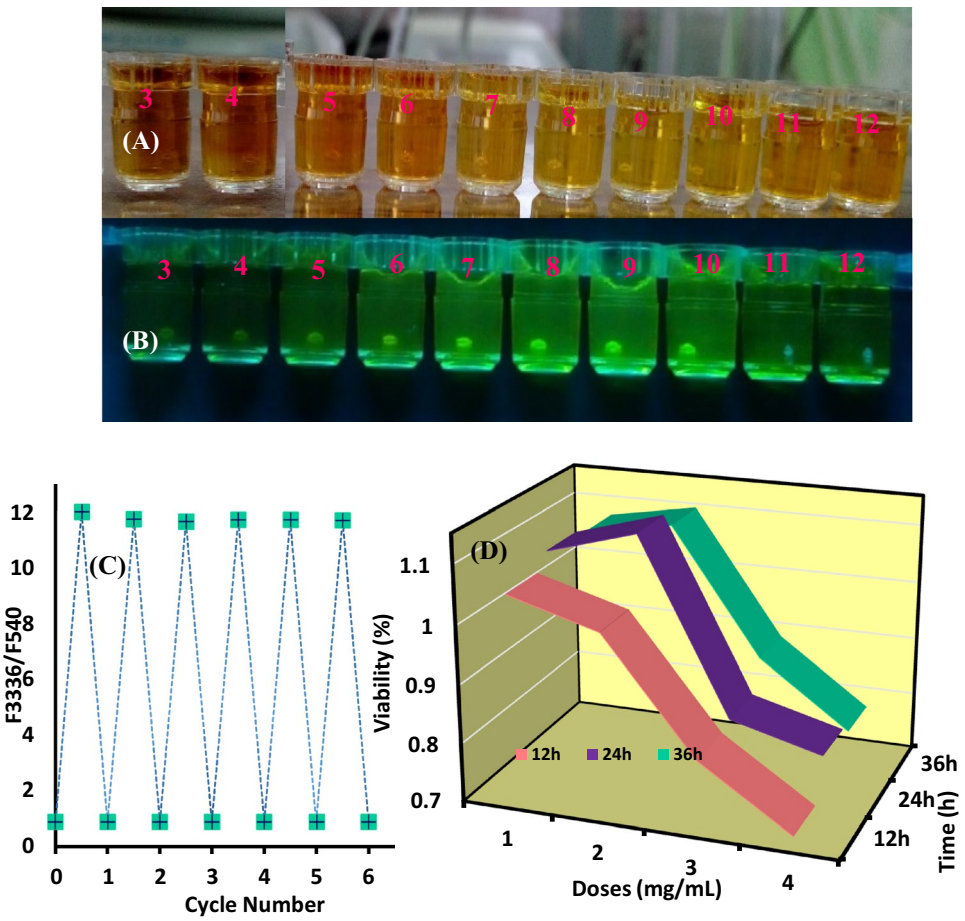

Fig. 4 Colorimetric profile of CDs solution at distinct pH at normal condition (**a**) and under UV (**b**) illumination (365 nm). **c** Growth inhibition assay (MTT) toward HeLa cells incubated with CDs (for low doses (1) 0.1 mg mL^{-1}), medium (2), (0.25 mg mL^{-1}), and high (3) doses (0.5 mg mL^{-1}) at different time intervals. **d** Reversible normalized PL ratio (F_{336}/F_{540}) changes of the CDs between pH 4.0 and pH 11.0 when pH varied with HCl and NaOH solutions repeatedly

of formed aggregations. The high pH sensitivity in PL properties of the CDs implies their surface state would be mostly responsible for their PL emission. As shown in Scheme 1a, based on FRET phenomenon for two active PL centers as donor (core) and acceptor (surface groups), the more probable mechanism may originate from protonation/deprotonation reactions of surface functional groups. The reason for this differential sensitivity may lie in the fact that the CDs are known to contain multiple emissive states that may respond differently toward different environmental conditions, which is pH change in this case. The presence of ionisable surface functional groups, like –COOH, –OH and $–NH_2$ as shown by FTIR, can generate surface states that may give rise to pH-sensitive emission wavelengths. The π-conjugated electron level governs the excitation [45, 46] wavelength of CDs, while the emission wavelength is affected by the vibration relaxation from surface functional groups [45, 46]. The remarkable effect of pH on the PL intensity in such a broad pH range indicates partly the overpowering presence of easily ionized $–NH_2$ and –COOH groups compared to C=O and–OH groups of CDs resulted in surface charge change due to protonation–deprotonation. We found this result very interesting, though the exact mechanism of this pH sensitivity is apart from the outlook of this article and presently under study.

MTT assay

For further biological application, we first evaluated CDs cytotoxicity toward HeLa cells using a standard MTT colorimetric assay. These cell lines incubated with the CDs at a higher dosage of 0.5 mg mL^{-1} than that used for bioimaging in live cells, for 12, 24 and 48 h, showed cellular viabilities (was more than 95% below 0.01 mg mL^{-1} and more than 85% even at a high concentration of 0.4 mg mL^{-1} of CDs) (Fig. 4d), demonstrating that the CDs are low toxic for live cells.

Cellular imaging and biosensing of pH in fixed and living cells

In order to probing the reactivity of the CD-based nanoprobes in a cell system, we explore the intracellular pH measurement on nigericin (used for homogenizing the intracellular pH and culture medium)-treated HeLa and MDA-MB-231 cells. Then, to explore the intracellular pH

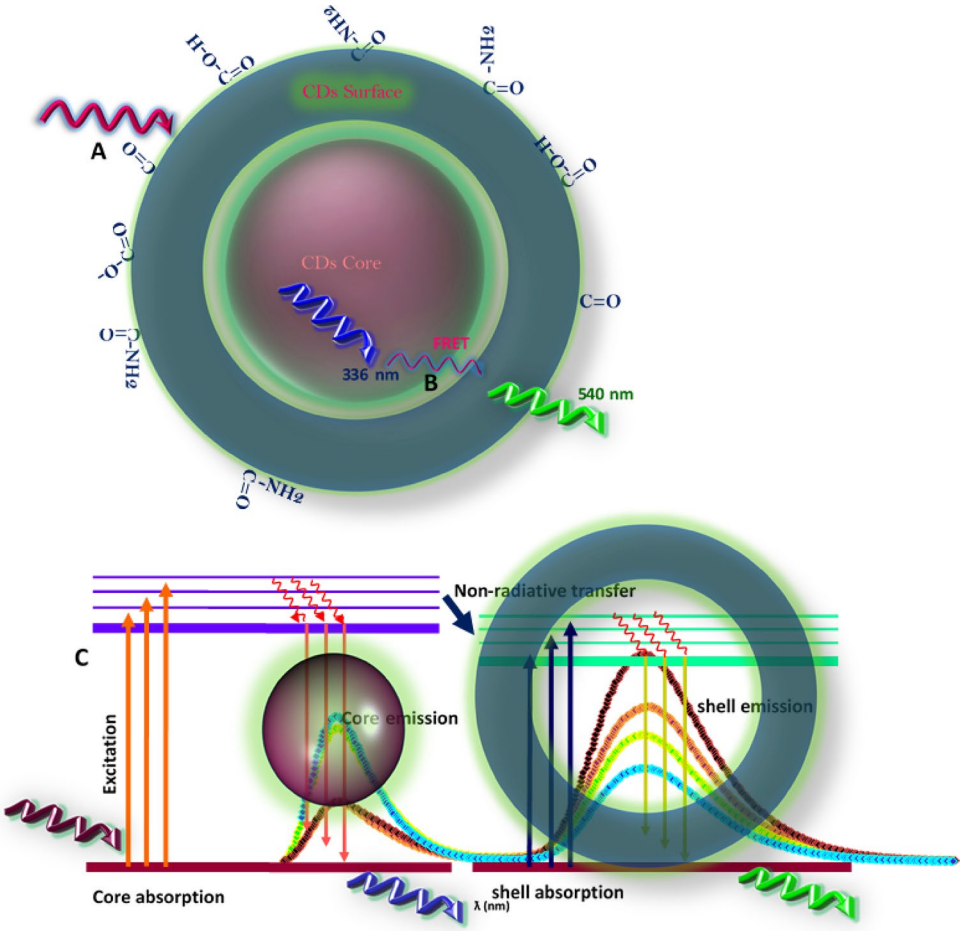

Scheme 1 The scheme shows the underlying possible emission mechanism in dual PL center CDs

sensing capabilities of the as-synthesized CDs, we incubated live MDA-MB-231 and HeLa cells with CDs for 30 min followed by a washing step and observed the internalization of the CDs. For fixed cells, by titrating the PBS with NaOH or HCl solutions (0.1 M) the pH was changed. Then, 15 min after titration solution addition, the images of the cells have been obtained under identical excitation and collection conditions. The obtained changes for I_{blue}/I_{green} and I_{blue}/I_{red}, indicate progressive dimming, the blue PL of CDs, and their interactions with the cell membrane, according to standard calibration curve for cell-free system. The fluorescence images of the HeLa cells stained with CDs overlaid with their respective bright field are shown in Fig. 5a. In comparison of fixation methods toward living cell imaging, fixation has advantages such as protection of morphology and tissues from bio-degradation; there are some disadvantages as fixation will break off some chemical process inside the cell and alter chemical environment regarding that in living sample. In Figs. 5b and 6a, we show confocal images of a living HeLa and MDA-MB-231 cell stained with CDs 15 min after the exposure to a 3.0×10^{-6} mM nigericin solution, to homogenize the surrounding medium using the H^+/K^+, overlaid with the respective bright-field pictures. The cells were observed to have a remarkable strong intracellular blue, green and red fluorescence emission when imaged under different channels, indicating that the CDs were readily taken up by the cells (Figs. 5b, 6a).

Ratiometric responses to pH

According to the color changes in cell images, the general trends of the average intracellular pH upon increment of pHs values, in agreement with its expected for two different cell lines, show the progressive enhancement of the green and red emission with exposure pHs, while the PL of cores did not change or diminish by elevating the pHs values.

This suggests that a ratiometric sensor can be constructed using both blue and green fluorescence as reporting signal. As depicted in Figs. 5b and 6a, the bright-field imaging reflects the state of cells survival and further confirms that the prepared CDs display good biocompatibility. The obtained images in Fig. 6a clearly show a high-contrast fluorescence image of CDs distributed around cytoplasm. Figure 6a also shows that the fluorescence signals are from the perinuclear regions of the cytosol, indicating that the CDs can label both the cell membrane and the nucleus of MDA-MB-231 cells. The different channel fluorescence intensities showed that the CDs can work in the physiological and extreme acidic and basic pH conditions. For confirming the importance of CDs pH response, the PL ratio curves of (I_{green}/I_{blue}) and (I_{red}/I_{blue}) versus pH of MDA-MB-231 cells were recorded (Fig. 6b, c), using RGB Color Picker software (installed on HTC camera cellphone). The images were

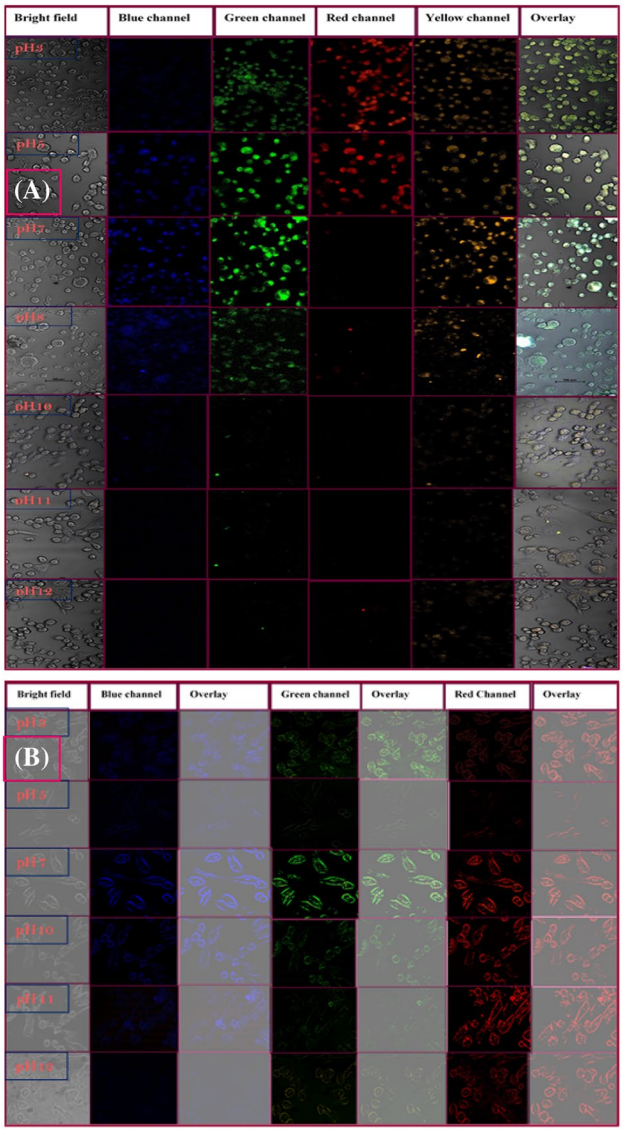

Fig. 5 **a** Confocal images of fixed Hela cells stained with CDs (2.5 μg mL^{-1}) at increasing pHs collected under 4 excitations, overlay of confocal images and bright-field images. The scale bar is 25 μm for all panels. **b** Confocal fluorescence images of living HeLa cells incubating with 0.05 mg mL^{-1} CDs in the presence of nigericin at different pHs value. Scale bar represents 25 μm. The fluorescence images of first, second, and third column were collected in blue channel (430–490 nm, λex = 365 nm), green channel (500–550 nm, λex = 405 nm), and red channel (650–700 nm, λex = 635 nm)

collected using the blue, green and red detector channels of the confocal microscope (Fig. 6b, c). These sets of data show the progressive emergence of the green and red luminescence by increasing pH (pH interval from 2.0 to 12.0), in agreement with the sensing behavior observed in the ensemble measurements. The color ratio of emitting spots in different pHs values was measured and plotted versus pH changes which yielded a linear graph. The fluorescence intensity was quantified for each image using Color Picker software. As

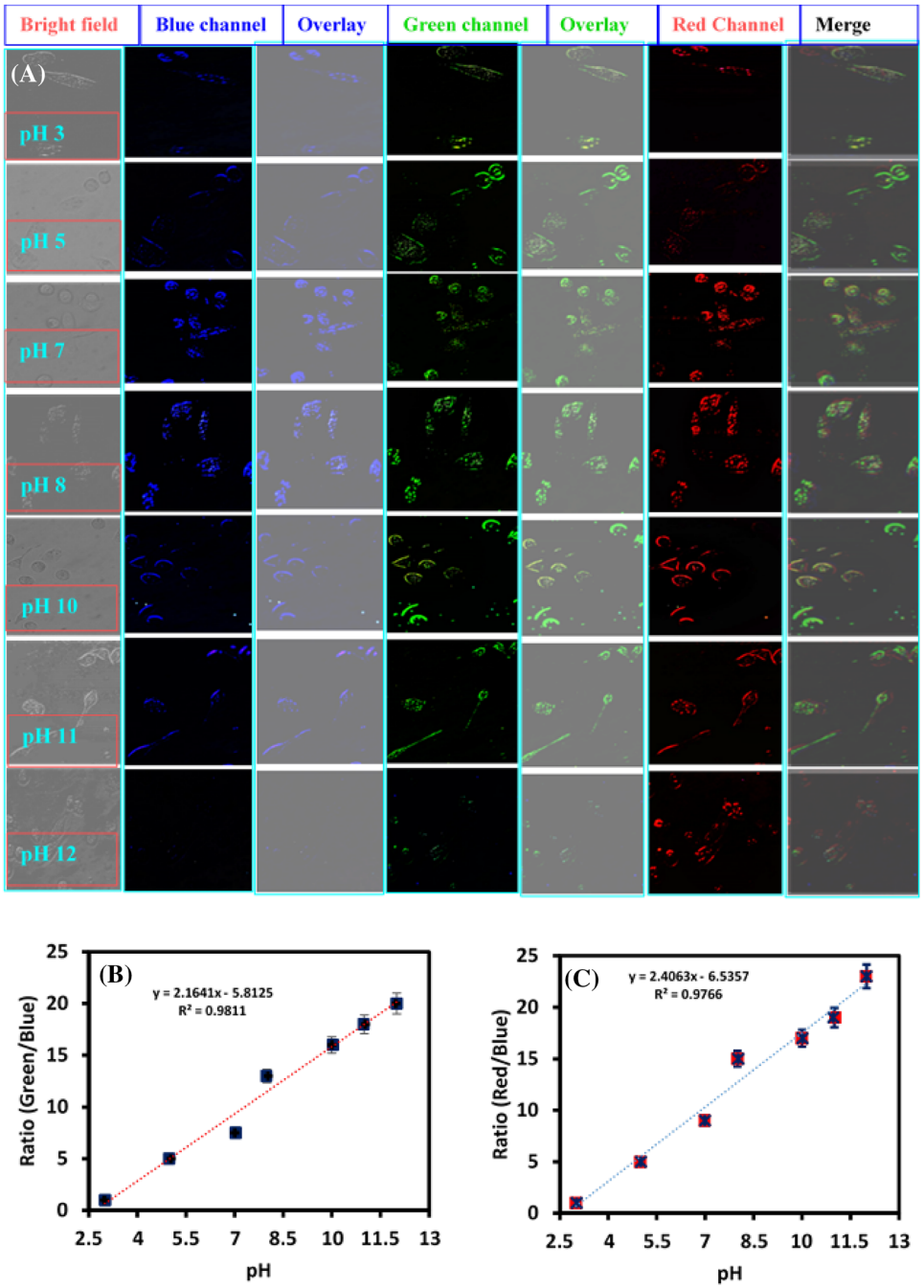

Fig. 6 **a** Confocal fluorescence images of living MDA-MB-231 cells incubating with 0.05 mg mL^{-1} CDs in the presence of nigericin at different PHs value. Scale bar represents 25 µm. The fluorescence images of first, second, and third column were collected in blue channel (430–490 nm, $\lambda ex = 365$ nm), green channel (500–550 nm, $\lambda ex = 405$ nm), and red channel (650–700 nm, $\lambda ex = 635$ nm). **b**, **c** Calibration curve of intracellular pH sensing by using CDs probe for MDA-MB-231 cells in term of ratio of PL emission intensity (I_{green}/I_{blue}) and (I_{red}/I_{blue}) versus pH. The data are expressed as the mean ± SD of three separate measurements

illustrated in Fig. 6b, the average fluorescence intensity ratio of I_{red}/I_{blue}, increased with the increasing pH values.

Conclusion

In summary, a simple method for synthesis of CDs with unique optical properties and its application as probe for ratiometric sensing of pH was developed. The dual fluorescence intensities (I_{336} nm/I_{540} nm) changed during pH changing from 2.5 to 12.0. Furthermore, the biocompatibility and highly brightness of the CDs are inherent advantages of ratiometric sensing. The proposed CDs used not only as feasible probe for pH sensing ratiometrically, but also they can be used in bioimaging. Since the proposed pH sensor features favorable photostability and low cytotoxicity in broad pH detection range (ca. 2.5–12), it can be used for long-term visualization of pH dynamic changes in living cells. The intracellular pH sensing has been demonstrated through confocal measurements on fixed and living HeLa and MDA-MB-231 cells in controlled pH conditions. We expect that the outstanding brightness, little or no toxicity and emission

characteristics of CDs probes, will greatly simplify detection of pH with low-cost portable fluorescence detection instruments, which is of highest importance for early detection of diseases in point of care diagnostics.

Acknowledgements This work was supported by Research Office of University of Kurdistan (Grant No. 4.1261) and Iranian Nanotechnology Initiative (Grant No. 142565).

References

1. W. Gao, H. Song, X. Wang, X. Liu, X. Pang, Y. Zhou, B. Gao, X. Peng, Carbon dots with red emission for sensing of Pt2+, Au3+ and Pd2+ and their bio-applications in vitro and in vivo. ACS Appl. Mater. Interfaces **10**, 1147–1154 (2018)
2. S. Mohamadi, A. Salimi, S. Hamd-Ghadareh, F. Fathi, S. Solemani, A FRET immunosensor for sensitive detection of CA 15-3 tumor marker in human serum sample and breast cancer cells using antibody functionalized luminescent carbon-dots and AuNPs-dendrimer aptamer as donor-acceptor pair. Anal. Biochem. **557**, 18–26 (2018)
3. S. Hamd-Ghadareh, A. Salimi, S. Parsa, F. Fathi, Simultaneous biosensing of CA125 and CA15-3 tumor markers and imaging of OVCAR-3 and MCF-7 cells lines via bi-color FRET phenomenon using dual blue-green luminescent carbon dots with single excitation wavelength. Int. J. Biol. Macromol. **118**, 617–626 (2018)
4. Z.C. Yang, M. Wang, A.M. Yong, S.Y. Wong, X.H. Zhang, H. Tan, A.Y. Chang, X. Li, J. Wang, Intrinsically fluorescent carbon dots with tunable emission derived from hydrothermal treatment of glucose in the presence of monopotassium phosphate. Chem. Commun. **47**, 11615–11617 (2011)
5. Y. Xiong, J. Schneider, C.J. Reckmeier, H. Huang, P. Kasákb, A.L. Rogach, Carbonization conditions influence the emission characteristics and the stability against photobleaching of nitrogen doped carbon dots. Nanoscale **9**, 11730–11738 (2017)
6. S. Hamd-Ghadareh, A. Salimi, F. Fathi, S. Bahrami, An amplified comparative fluorescence resonance energy transfer immunosensing of CA125 tumor marker and ovarian cancer cells sing green and economic carbon dots for bio-applications in labeling, imaging and sensing. Biosens. Bioelectron. **96**, 308–316 (2017)
7. S. Hamd Qaddare, A. Salimi, Amplified fluorescent sensing of DNA using luminescent arbon dots and AuNPs/GO as a sensing platform: a novel coupling of FRET and DNA hybridization for homogeneous HIV-1 gene detection at femtomolar level. Biosens. Bioelectron. **89**, 773–780 (2017)
8. P. Khramtsov, M. Kropaneva, T. Kalashnikova, M. Bochkova, V. Imganova, S. Zamorina, M. Rayev, Highly stable conjugates of carbon nanoparticles with DNA aptamers. Langmuir **34**, 10321–10332 (2018)
9. J. He, Y. He, Y. Chen, X. Zhang, C. Hu, J. Zhuang, B. Lei, Y. Liu, Construction and multifunctional applications of carbon dots/PVA nanofibers with phosphorescence and thermally activated delayed fluorescence. Chem. Eng. J. **347**, 505–513 (2018)
10. N.L. Teradal, R. Jelinek, Carbon nanomaterials in biological studies and biomedicine. Adv. Healthc. Mater. **6**, 1700574 (2017)
11. H. Feng, Z. Qian, Functional carbon quantum dots: a versatile platform for chemosensing and biosensing. Chem. Rec. **17**, 1–16 (2017)
12. K. Jiang, S. Sun, L. Zhang, Y. Lu, A. Wu, C. Cai, H. Lin, Red, green, and blue luminescence by carbon dots: full-color emission tuning and multicolor cellular imaging. Angew. Chem. Int. Ed. **54**, 5360–5453 (2015)
13. B.C. Martindale, G.A.M. Hutton, C.A. Caputo, S. Prant, R. Godin, J.R. Durrant, E. Reisner, Enhancing light absorption and charge transfer efficiency in carbon dots through graphitization and core nitrogen doping. Angew. Chem. **56**, 6459–6463 (2017)
14. S. Hu, X. Meng, F. Tian, W. Yang, N. Li, C. Xue, J. Yang, Q. Chang, Dual photoluminescence centers from inorganic-salt-functionalized carbon dots for ratiometric pH sensing. J. Mater. Chem. C **5**, 9849–9853 (2017)
15. H. Ding, S.B. Yu, J.S. Wei, H.M. Xiong, Full-color light-emitting carbon dots with a surface-state-controlled luminescence mechanism. ACS Nano **10**, 484–491 (2016)
16. X. Meng, Q. Chang, C. Xue, J. Yang, S. Hu, Full-colour carbon dots: from energy-efficient synthesis to concentration-dependent photoluminescence properties. Chem. Commun. **53**, 3074–3077 (2017)
17. R. Mohan, J. Drbohlavova, J. Hubalek, Dual band emission in carbon dots. J. Phys. Lett. **692**, 196–201 (2018)
18. L. Wang, S.J. Zhu, H.Y. Wang, S.N. Qu, Y.L. Zhang, J.H. Zhang, Q.D. Chen, H.L. Xu, W. Han, B. Yang, H.B. Sun, Common origin of green luminescence in carbon nanodots and graphene quantum dots. ACS Nano **8**, 2541–2547 (2014)
19. W. Cheng, J. Xu, Z. Guo, D. Yang, X. Chen, W. Yan, P. Miao, Hydrothermal synthesis of N, S co-doped carbon nanodots for highly selective detection of living cancer cells. J. Mater. Chem. B **6**, 5775–5780 (2018)
20. H. Wang, X. Sun, T. Zhang, X. Chen, J. Zhu, W. Xu, X. Bai, B. Dong, H. Cui, H. Song, Photoluminescence enhancement of carbon dots induced by hybrids of photonic crystals and gold–silver alloy nanoparticles. J. Mater. Chem. C **6**, 147–152 (2018)
21. X. Sun, C. Bruckner, Y. Lei, One-pot and ultrafast synthesis of nitrogen and phosphorus co-doped carbon dots possessing bright dual wavelength fluorescence emission. Nanoscale **17**, 17278–17282 (2017)
22. Y. Wang, D. Shan, G. Wu, H. Wang, F. Ru, X. Zhang, L. Li, Y. Qian, X. Lu, A. Novel, "Dual-potential" ratiometric electrochemiluminescence DNA sensor based on enhancing and quenching effect by G-quadruplex/hemin and Au-luminol bifunctional nanoparticles. Biosens. Bioelectron. **106**, 64–70 (2018)
23. V. Nguyen, L. Yan, H. Xu, M. Yue, One-step synthesis of multi-emission carbon nanodots for ratiometric temperature sensing. Appl. Surf. Sci. **427**, 1118–1123 (2018)
24. W. Song, W. Duan, Y. Liu, Z. Ye, Y. Chen, H. Chen, S. Qi, J. Wu, D. Liu, L. Xiao, C. Ren, X. Chen, Ratiometric detection of intracellular lysine and pH with one-pot synthesized dual emissive carbon dots. Anal. Chem. **89**, 13626–13633 (2017)
25. Y. Zhang, S. Li, Z. Zhao, Using nanoliposomes to construct a FRET-based ratiometric fluorescent probe for sensing intracellular pH values. Anal. Chem. **88**, 12380–12385 (2016)
26. X. Lu, J. Zhang, Y.N. Xie, X. Zhang, X. Jiang, X. Hou, P. Wu, Ratiometric phosphorescent probe for thallium in serum, water, and soil samples based on long-lived, spectrally resolved, Mn-doped ZnSe quantum dots and carbon dots. Anal. Chem. **90**, 2939–2945 (2018)
27. J. Huang, L. Ying, X. Yang, Y. Yang, K. Quan, H. Wang, N. Xie, M. Qu, Q. Zhou, K. Wang, Ratiometric fluorescent sensing of pH values in living cells by dual-fluorophore-labeled i-motif nanoprobes. Anal. Chem. **87**, 8724–8731 (2015)
28. Q. Yang, Z. Ye, M. Zhong, B. Chen, J. Chen, R. Zeng, L. Wei, H.W. Li, L. Xia, Self-assembled fluorescent bovine serum albumin nanoprobes for ratiometric pH measurement inside living cells. ACS Appl. Mater. Interfaces **8**, 9629–9634 (2016)
29. F.W. Pratiwi, C.H. Hsia, C.W. Kuo, S.M. Yang, Y.K. Hwu, P. Chen, Construction of single fluorophore ratiometric pH sensors using dual-emission Mn^{2+}-doped quantum dots. Biosens. Bioelectron. **84**, 133–140 (2016)

30. Z.M. Ying, Z. Wu, B. Tu, W. Tan, J.H. Jiang, Genetically encoded fluorescent RNA sensor for ratiometric imaging of MicroRNA in living tumor cells. J. Am. Chem. Soc. **139**, 9779–9782 (2017)
31. H. Li, H. Dong, M. Yu, C. Liu, Z. Li, L. Wei, L. Sun, H. Zhang, NIR ratiometric luminescence detection of pH fluctuation in living cells with hemicyanine derivative-assembled upconversion nanophosphors. Anal. Chem. **89**, 8863–8869 (2017)
32. X. Zhu, M. Xiong, H. Liu, G. Mao, L. Zhou, H. Zhang, X. Hu, X. Zhang, W.A. Tan, FRET-based ratiometric two-photon fluorescent probe for dual-channel imaging of nitroxyl in living cells and tissues. Chem. Commun. **52**, 733–736 (2016)
33. W. Wang, J. Xia, J. Feng, M. He, M. Chen, H. Wang, Green preparation of carbon dots for intracellular pH sensing and multicolor live cell imaging. J. Mater. Chem. B **4**, 7130–7137 (2016)
34. A. Sharma, T. Gadly, A. Gupta, A. Ballal, S.K. Ghosh, M. Kumbhakar, Origin of excitation dependent fluorescence in carbon nanodots. J. Phys. Chem. Lett. **7**, 3695–3702 (2016)
35. X. Gong, W. Lu, Y. Liu, Z. Li, S. Shuang, C. Dong, M. Choi, Low temperature synthesis of phosphorous and nitrogen co-doped yellow fluorescent carbon dots for sensing and bioimaging. J. Mater. Chem. B **23**, 6813–6819 (2015)
36. W. Niu, L. Fan, M. Nan, Z. Li, D. Lu, M. Wong, S. Shuang, C. Dong, Ratiometric emission fluorescent pH probe for imaging of living cells in extreme acidity. Anal. Chem. **87**, 2788–2793 (2015)
37. X. Sun, C. Brückner, Y. Lei, One-pot and ultrafast synthesis of nitrogen and phosphorus co-doped carbon dots possessing bright dual wavelength fluorescence emission. Nanoscale **7**, 17278–17282 (2015)
38. L. Wang, H.S. Zhou, Green synthesis of luminescent nitrogen-doped carbon dots from milk and its imaging application. Anal. Chem. **86**, 8902–8905 (2014)
39. B. Zhi, M.J. Gallagher, M.B.P. Frank, T.Y. Lyons, T.A. Qiu, J. Da, A.C. Mensch, R.J. Hamers, Z. Rosenzweig, D.H. Fairbrother, C.L. Haynes, Investigation of phosphorous doping effects on polymeric carbon dots: fluorescence, photostability, and environmental impact. Carbon **129**, 438–449 (2018)
40. T. Feng, H.J. Chua, Y. Zhao, Carbon-dot-mediated co-administration of chemotherapeutic agents for reversing cisplatin resistance in cancer therapy. ACS Biomater. Sci. Eng. **3**, 1535–1541 (2017)
41. Y. Zhou, S. Sharma, Z. Peng, R. Leblanc, Polymers in carbon dots: a review. Polymers **9**, 67 (2017)
42. S. Amiri, R. Ahmadi, A. Salimi, A. Navaee, S. Hamd Qaddareh, M.K. Amini, Ultrasensitive and highly selective FRET aptasensor for Hg^{2+} measurement in fish samples using carbon dots/AuNPs as donor/acceptor platform. New J. Chem. **42**, 16027–16035 (2018)
43. S. Mohammadi, A. Salimi, Fluorometric determination of microRNA-155 in cancer cells based on carbon dots and MnO_2 nanosheets as a donor-acceptor pair. Microchim. Acta **185**, 372 (2018)
44. M. Pirsaheb, S. Mohammadi, A. Salimi, M. Payandeh, Functionalized fluorescent carbon nanostructures for targeted imaging of cancer cells: a review. Microchim. Acta **186**, 231 (2019)
45. M. Havrdova, K. Hola, J. Skopalik, K. Tomankova, M. Petr, K. Cepe, K. Polakova, J. Tucek, A.B. Bourlinos, R. Zboril, Toxicity of carbon dots—effect of surface functionalization on the cell viability, reactive oxygen species generation and cell cycle. Carbon **99**, 238–248 (2016)
46. B.B. Chen, M.L. Liu, L. Zhan, C.M. Li, C. Huang, Terbium (III) modified fluorescent carbon dots for highly selective and sensitive ratiometry of stringent. Anal. Chem. **90**, 4003–4009 (2018)